Noise and vibration of permanent magnet synchronous electric motors: A simplified analytical model

Federico Ballo, Massimiliano Gobbi, Gianpiero Mastinu, and Roberto Palazzetti

***Abstract*—Design of electric motors, especially for automotive applications where early design choices have significant impacts on the final results, in terms of both cost and performances, is a matter of primary importance, with direct consequences on the entire vehicle. Common practice lacks of simple, yet reliable, analytical method to evaluate vibration and noise emission of permanent magnet synchronous motors (PMSMs), and this is the gap that the work here proposed aims to fill. In particular, electric vehicles noise requirements have added a design opportunity to manufacturers, that, depending on the type of costumers they are selling their products to, need to comply with different preferences. Accurately estimate noise emissions of such complex machines is a difficult matter, that can be fully exploited only at the end of the design process. The paper aims to provide a simple, yet accurate enough, tool to estimate the noise emission of electrical motors at the early stage of the design, giving engineers and researchers a tool to drive their choices. An equivalent curved beam model is employed for modelling the structural vibration of the stator when subjected to electromagnetic forces. The sound pressure amplitudes are analytically derived based on the acoustic solution for infinitely long cylindrical radiators. Part of the innovation lays on the fact that the contributions of both radial and tangential forces are taken into account, and a discussion on the effect and influence of the latter on the stator acoustic emission is presented. The sound pressure radiated from the outer surface of the stator is calculated, and a unique indicator of sound emission, named Sound Pressure Level (SPL), is determined. The proposed method is validated against data of two PMSMs from literature, showing good agreement with experiments, proving the method is a reliable tool for electric motor designers to be used especially during the early stage of design.**

***Index Terms*—Analytical method, vibration, noise, permanent magnet, synchronous motors**

I. Introduction

On 14th of July 2021, the European Commission stated the targets for mobility in EU [1]. The proposed deadline for banning internal combustion engines from the market was set to 2035. This unprecedented shift of technology - from conventional to electric powertrains - will drag the R&I (Research and Innovation) investments of European automotive industry towards electric vehicles. Nearly 50 billion euro/year is the budget for R&I in the automotive sector in EU alone [2], [3]; in US and China the market of electric vehicles is growing fast with ambitious targets [4]. The rising interest of the automotive industry on electric drives provides a number of new aspects that designers have to consider, investigate, and improve, among which noise of motors plays a relevant role. One of the main features of electric motors is their noiselessness, especially when compared to their internal combustion counterparts. Automotive manufacturers face different needs when dealing with electric motors noise, mainly depending on the type of vehicle: low-segment car manufacturers generally look for noiseless motors, whereas sport or luxury cars, generally hybrid, are required to produce a noise to give the drivers the feel of the power of their engine. In both cases, the acoustic emission of electric motors is a matter of rising importance. According to the literature, three main distinctive approaches are employed for noise and vibration modelling of PMSMs, namely numerical, analytical and semi-analytical methods [5], [6].

Most of the work found in literature about Noise Vibration and Harshness (NVH) modelling of electric motors [7]–[14] makes use of finite element software.

In their work, Lin et al. [9] propose a multiphysics model for electromagnetic vibration and noise calculation, based on a finite elements model that computes the forces acting on the motor's stator. Their interest lays in the effect of current harmonics on vibration and noise, concluding that phase angle, phase sequence, and frequency of current harmonics should be considered. The same authors, in a different paper [14], propose a multiphysics model to predict electromagnetic noise, and analyze sound quality of a permanent magnet synchronous motor (PMSM) within a variable speed range. They validate their model with experiments comparing four indexes: Sound Pressure Level (SPL), Loudness level, Sharpness, and Fluctuation Strength and Roughness, showing very good agreement. Torregrossa et al. [13], similarly, use SPL to validate their multi-physical numerical model against experiments, and found very accurate results in terms of estimation of noise and vibrations.

Despite the high level of accuracy that such models can achieve, their main drawback is the need of complex softwares, that, especially at the early stage of design, might result expensive in terms of time and computational costs. Additionally, complex and detailed numerical models require the tuning of a large set of input parameters related to motor geometry, materials and modal dynamics [15]–[17], which may not be readily available, especially at an early design stage.

Simplified models, on the other hand, require a limited

F. Ballo, M. Gobbi, G. Mastinu and R. Palazzetti are with the Mechanical Engineering Department, Politecnico di Milano, Milan, 20156, Italy (e-mail: federicomaria.ballo@polimi.it, massimiliano.gobbi@polimi.it, gianpiero.mastinu@polimi.it, roberto.palazzetti@polimi.it .

This paper was produced by the IEEE Publication Technology Group.
Manuscript received ????? ??, 2022; revised ????? ??, 2022.

computational and implementation effort, at the price of lower accuracy and level of detail. Indeed, such kind of approaches represent valuable tools to help designers to steer the design process towards high quality products and keep critical decisions at an early stage of the process.

One of the few fully analytical works on NVH modelling of electric motors was published by Weilharter et al. [18]: the authors propose and validate a comprehensive analytical approach to determine the noise behavior of coiled rotors induction machines. Analytical expressions of the electromagnetic forces in the air-gap are employed, and the approach is based on space-and-time harmonic decomposition of the Maxwell stress tensor. The radial vibration and acoustic emission of the stator surface is then computed by means of analytical formulae based on an equivalent ring model and cylindrical sound radiator, respectively.
A similar method is proposed by Gieras et al. [19], who adopt a lumped system analysis approach to include the effect of teeth, windings and polymer insulation in the structural vibration of the ring.

Islam et al. [20] in their work exploit the analytical solution of an elastic hollow disc subject to internal pressure to compute displacement and noise of the stator body. A remarkable result is presented in [21], where the authors propose a double-layer cylindrical shell orthotropic model to calculate the radial vibration of the stator core of an electric machine. In the paper, analytical solutions for eigenfrequencies and forced vibration are derived.

It is important to notice that all the above mentioned models neglect the effect of tangential electromagnetic forces on the structural vibration of the machine, despite their importance and effect when dealing with noise emitted by induction motors is still an open topic among the scientific community. Discordant opinions have been found; a large amount of the literature agrees in neglecting tangential effects, mainly because of radial forces are often larger, and because of analytical methods are difficult to implement while considering the deflection caused by tangential forces [10].

On the other hand, there exists some studies leading to opposite results; Boesing et al. [22] show that tangential forces should generally be included, as their effect can not be neglected a priori. Lan et al. [10] provide a deeper investigation on the impact of tangential forces, suggesting that a number of architectural parameters of the motor have effect on whether tangential forces are relevant, for example long thin teeth lead to strong lever arm effect and not so small force amplitudes as commonly expected, resulting in the contribution of tangential force to the final vibration comparable to that of radial forces.

Xu et al. [23], recently developed a simplified analytical framework for deriving the dynamic equations of the radial vibration of Permanent Magnets (PM) machines, considering the effect of tangential forces, as well as that of magnetostriction and tooth/slot geometry. However, the equations are solved by numerical integration and the analysis is limited to the vibrational behaviour only.

In the present paper, an analytical simplified model for the NVH simulation of PM electric motors is proposed. The proposed analytical model is based on a curved elastic beam, whose structural and inertial parameters are derived from the physical and geometrical properties of stator core and external case. The work aims at covering some of the highlighted gaps found in the literature - the major contributions and novelties are listed as follows.

- Explicit, unreferenced closed-form expressions of forced vibration and sound pressure field radiated from the motor structure are derived. The derived mathematical expressions include the effect of tangential electromagnetic forces and the lever-arm effect introduced by the tooth, generally neglected in state of the art analytical methods.
- The simple and compact expressions provide useful insights on NVH behaviour of electrical machines, as clear and immediate relation between basic structural and topological parameters of the machine and NVH performances are established.
- The method is meant to be used as a prompt and quick tool for supporting engineers to address critical decisions at early stages of the design process.

The paper is structured as follows. In Sec. II, numerical electromagnetic model and forces exciting the stator structure are described. In Sec. III, the analytical model for vibration and acoustic sound pressure calculation is described in detail. Experimental validation and acoustic analysis are addressed in Sec. IV. Obtained results and applicability of the method are discussed in Sec. V, while concluding remarks are drawn in Sec. VI.

II. Electromagnetic forces

In this paper, two different electric motors are considered to test the capabilities of the proposed analytical approach. The first one, denoted as Motor 1, is the 10-pole/12-slot surface-mounted PMSM studied in [10]. For this motor, a numerical model has been implemented in ANSYS Motorcad® software, to derive the electromagnetic forces acting on the stator core. The numerical model here developed has been validated against the prototype shown in [10] matching the phase currents of the given speed. The second motor (i.e. Motor 2) here used to benchmark the proposed approach is the prototype of a PMS electric machine presented in [24]: it features the same 10-poles/12-slot topology of the former, and was specifically realised to provide benchmark data for electromagnetic-induced vibrations [24]. For this second motor, the open-circuit air gap stress harmonics computed in [24] have been employed. Such forces have been validated by means of specific tests with a search coil magnetometer wounded around the stator tooth as described in [24]. The main parameters of the two considered motors are summarised in TABLE I

TABLE I
PARAMETERS OF THE TWO INVESTIGATED 10-POLE/12-SLOT PMSMS

Parameter description	Motor 1 [10]	Motor 2 [24]	Units
Rated power	4	-	kW
Rated current	23.5	-	A
Rated line voltage	112	-	V
Rated torque	26.5	-	Nm
Rated speed	1440	0-5000	rpm
Remanence	1.2	1.28	T
Relative permeability	1.05	1.05	-
PM thickness	3.5	5	mm
Active length	106	140	mm
Stator bore diameter	75	96	mm
Tooth width	9.6	12	mm
Slot depth	19.4	20	mm
Copper slot fill	0.57	-	-
Case outer diameter	140	-	mm
Case thickness	7.5	-	mm

The electromagnetic force density acting at the air-gap is calculated from the Maxwell stress tensor as [25]

$$\sigma_{\mathrm{r}}(\theta,t) = \frac{1}{2\mu_0}\left(B_{\mathrm{r}}(\theta,t)^2 - B_{\tau}(\theta,t)^2\right) \tag{1a}$$

$$\sigma_{\mathrm{t}}(\theta,t) = \frac{1}{\mu_0} B_{\mathrm{r}}(\theta,t)\, B_{\tau}(\theta,t) \tag{1b}$$

where σ_{r} and σ_{t} are the radial and tangential force density, respectively, μ_0 is the vacuum permeability, while B_{r} and B_{τ} are the radial and tangential components of the magnetic flux density, respectively, which are function of the stator angular position θ and time. Assuming a uniform distribution along the axial length of the stator L_{s}, the force density shown in eq. 1 can be decomposed into its time- and spatial- harmonic content [10], [19], [26] as

$$f(\theta,t) = \sigma_{\mathrm{r}} \cdot L_{\mathrm{s}} = \sum_{n=-\infty}^{+\infty}\sum_{k=-\infty}^{+\infty} F_{n,k} \cdot e^{i(n\theta + k\omega_0 t)} \tag{2a}$$

$$p(\theta,t) = \sigma_{\mathrm{t}} \cdot L_{\mathrm{s}} = \sum_{n=-\infty}^{+\infty}\sum_{k=-\infty}^{+\infty} P_{n,k} \cdot e^{i(n\theta + k\omega_0 t)} \tag{2b}$$

where f and p are forces per unit of length (N/m), n and k are the space- and time- order of the harmonic, respectively, $F_{n,k}$ and $P_{n,k}$ are the (n,k) harmonic amplitude and ω_0 is the fundamental electric frequency, related to the motor mechanical speed Ω and to the number of pole pairs κ

$$\Omega = \frac{\omega_0}{\kappa} \tag{3}$$

A. Forces of Motor 1

The obtained spectra of the magnetic force densities of the machine by [10] with the motor running at 26 Nm and 1440 rpm are depicted in Fig. 1. For both radial (Fig. 1a) and tangential (Fig. 1b) force distributions, the main contribution is given by the (2,2) and (10,2) harmonic waves, a result consistent with that found in [10].

Fig. 2 shows the tooth lumped radial (Fig. 2a) and tangential (Fig. 2b) force waveforms over an electric cycle.

B. Forces of Motor 2

The 2D spectra of radial and tangential force densities of Motor 2 computed by means of numerical simulation under open circuit condition are shown in Fig. 4a and Fig. 4b respectively. In this case numerical results have been kindly provided by the authors of [24]. Similarly to Motor 1 (Fig. 1), the dominant contribution is given by (10,2) and (2,2) harmonic waves, typical of this motor topology. Moreover, the amplitude of tangential forces is comparable to that of radial ones, as clearly highlighted by the radial and tangential waveforms computed at 550 rpm (Fig. 3a and Fig. 3b respectively).

III. ANALYTICAL MODEL FOR NOISE AND VIBRATION PREDICTION

Fig. 5a sketches the simplified geometry of the stator core and the electromagnetic force distribution acting on the teeth. This structure is approximated by the curved beam of Fig. 5b, where R is the radius of the neutral axis, the product $E \cdot J$ is the equivalent bending stiffness, ρ and A the density and cross sectional area of the beam, respectively.

The electromagnetic radial and tangential force distributions of Fig. 5a are moved from the tooth surfaces to the beam neutral axis and the new terms $\bar{f}$, $\bar{p}$, and q of Fig. 5b are computed as

$$\bar{f}(\theta,t) = f(\theta,t) \cdot \frac{2\pi R_b}{2\pi R} \tag{4a}$$

$$\bar{p}(\theta,t) = p(\theta,t) \cdot \frac{2\pi R_b}{2\pi R} \tag{4b}$$

$$q(\theta,t) = -p(\theta,t) \cdot \frac{2\pi R_b}{2\pi R} \cdot (R - R_b) \tag{4c}$$

where the term of eq. 4c is the distributed moment that accounts for the transportation of the tangential force from R_b to R (with sign depending on the chosen reference system).

A. Curved beam equivalent parameters

The parameters of the equivalent curved beam of Fig. 5b are derived from the main structural and geometrical parameters of the motor as follows.

At first, the radial structure of the motor is divided into the three main annular regions highlighted in Fig. 6, namely the inner region (modelling teeth and winding, noted with the subscript w), the mid region (the stator back iron, noted with the subscript y) and the outer region (the outer case of the actual motor, noted with the subscript h). Following the notation of Fig. 6, the radius R of the neutral axis of such a composite equivalent structure is computed as

$$R = \frac{E_{\mathrm{w}}A_{\mathrm{w}}R_{\mathrm{w}} + E_{\mathrm{y}}A_{\mathrm{y}}R_{\mathrm{y}} + E_{\mathrm{h}}A_{\mathrm{h}}R_{\mathrm{h}}}{E_{\mathrm{w}}A_{\mathrm{w}} + E_{\mathrm{y}}A_{\mathrm{y}} + E_{\mathrm{h}}A_{\mathrm{h}}} \tag{5}$$

where the terms $E_{\mathrm{i=w,y,h}}$, $A_{\mathrm{i=w,y,h}}$ and $R_{\mathrm{i=w,y,h}}$ on the right side are the elastic modulus, cross sectional area and mean radius of the three regions, respectively. The result of eq. 5 provides the reference radius of the equivalent ring of Fig. 5b. The term E_{w} in eq. 5 accounts for the combined effect of copper windings, polymer insulation and tooth body

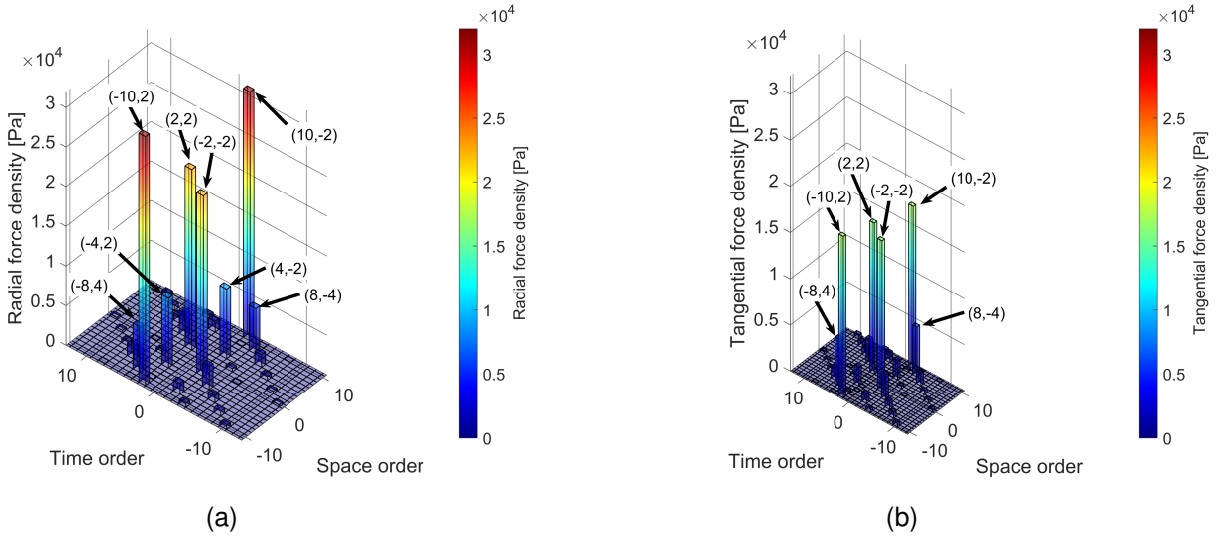

Fig. 1. Electromagnetic force spectra of Motor 1 at 26 Nm. (a) Radial force density. (b) Tangential force density.

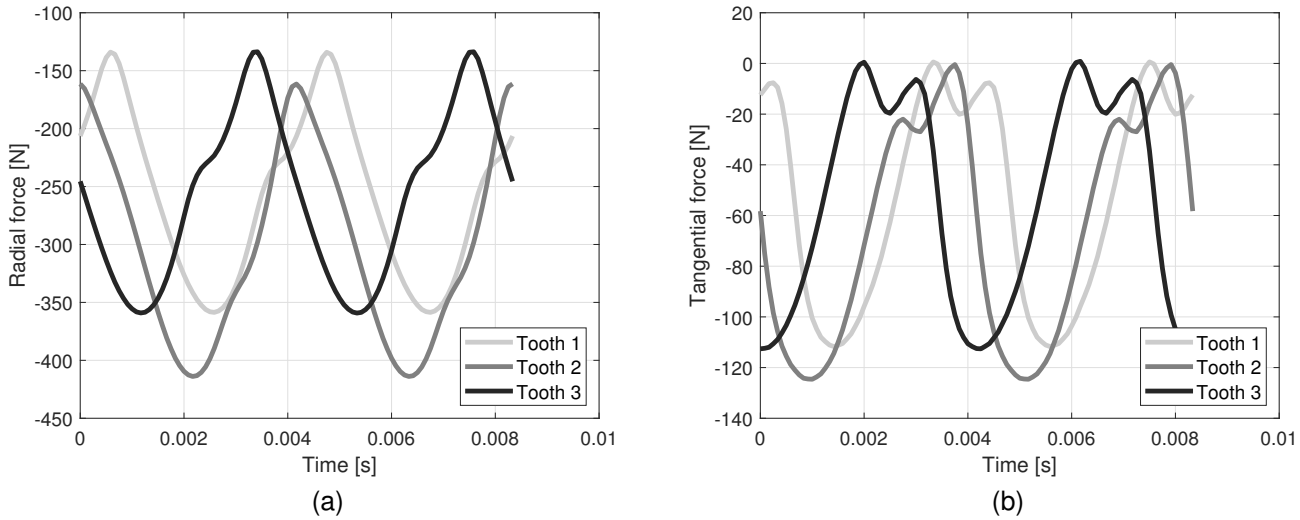

Fig. 2. Lumped tooth forces of Motor 1 at 26 Nm, 1440 rpm. (a) Radial force waveforms. (b) Tangential force waveforms.

- a reasonable estimation of this parameter can be obtained by applying the Reuss rule

$$\frac{1}{E_{\mathrm{w}}} = \frac{1}{E_{\mathrm{y}}}\frac{V_{\mathrm{teeth}}}{V_{\mathrm{TOT}}} + \frac{1}{E_{\mathrm{c}}}\frac{\alpha V_{\mathrm{slot}}}{V_{\mathrm{TOT}}} + \frac{1}{E_{\mathrm{ins}}}\frac{(1-\alpha)\,V_{\mathrm{slot}}}{V_{\mathrm{TOT}}} \tag{6}$$

where E_{y}, E_{c} and E_{ins} are Young's moduli of the materials of stator lamination, copper windings and polymer insulation, respectively, α is the copper slot fill, V_{teeth} and V_{slot} are the volumes of teeth and slots, respectively, and V_{TOT} is the total volume.

The bending stiffness EJ of the equivalent ring of Fig. 5b is finally set to obtain the same stiffness of the laminated structure of Fig. 6 and reads

$$\begin{aligned} EJ =& E_{\mathrm{w}}\left(J_{\mathrm{w}} + \gamma \cdot A_{\mathrm{w}} \cdot \Delta_{\mathrm{w}}^2\right) + E_{\mathrm{y}}\left(J_{\mathrm{y}} + \gamma \cdot A_{\mathrm{y}} \cdot \Delta_{\mathrm{y}}^2\right) + \\ & E_{\mathrm{h}}\left(J_{\mathrm{h}} + \gamma \cdot A_{\mathrm{h}} \cdot \Delta_{\mathrm{h}}^2\right) \end{aligned} \tag{7}$$

where J_{w}, J_{y} and J_{h} are the second moment of inertia around the centroidal axes of the three sections, respectively; Δ_{w}, Δ_{y} and Δ_{h} are the distances of the three centroidal axes from the neutral axis. The term γ in eq. 7 is a correction factor that accounts for the relative movement between the three rings in the hoop direction. This coefficient, equal to 0.4, applies only to mode orders higher than 2 and has been identified from experimental data on a set of different motor structures.

Finally, the mass of the ring is set equal to the actual motor's and reads

$$\rho \cdot A = \frac{m_{\mathrm{w}} + m_{\mathrm{ins}} + m_{\mathrm{teeth}} + m_{\mathrm{y}} + m_{\mathrm{h}}}{2\pi R} \tag{8}$$

where ρ and A are the mass density and the cross sectional area of the equivalent beam, respectively.

The structural and geometrical inputs of the model are listed in TABLE II.

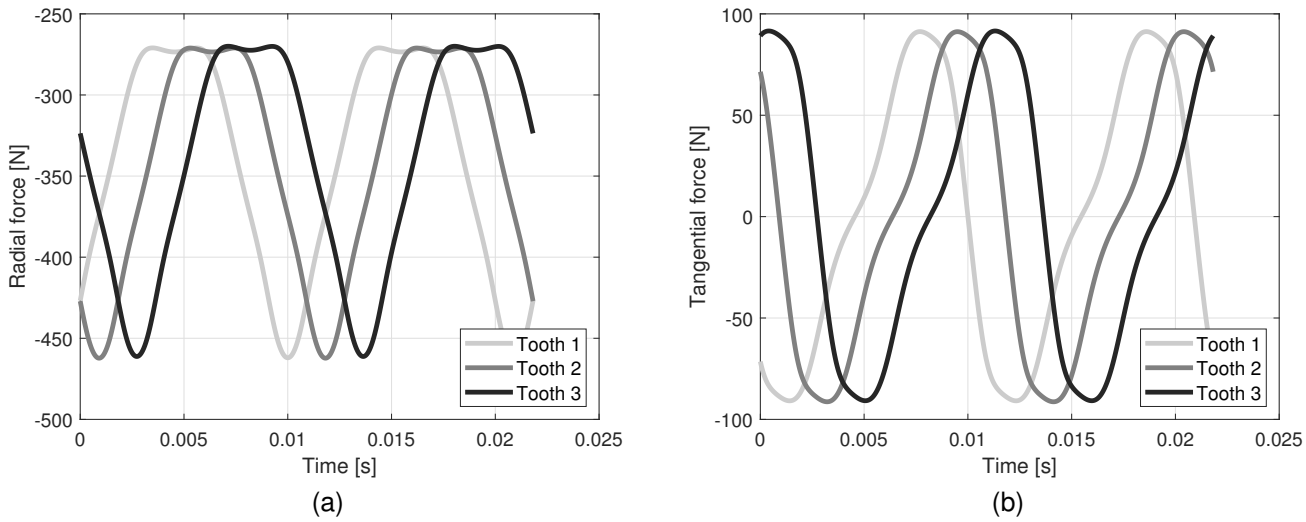

Fig. 3. Lumped tooth forces of Motor 2 at 550 rpm, open circuit condition. (a) Radial force waveforms. (b) Tangential force waveforms.

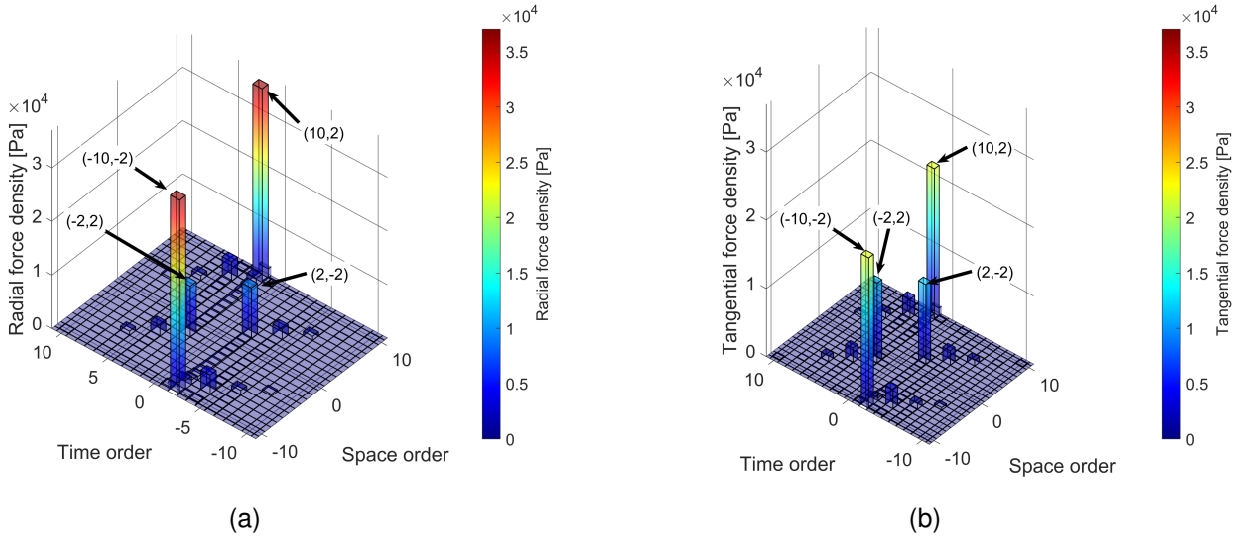

Fig. 4. Electromagnetic force spectra of Motor 2, open circuit test. (a) Radial force density. (b) Tangential force density.

TABLE II
ANALYTICAL MODEL PARAMETERS OF THE TWO INVESTIGATED 10-POLE/12-SLOT PMSMS

Parameter description	Symbol	Motor 1	Motor 2	Units
Beam cross sectional area	A	$5.936 \cdot 10^{-4}$	$7.8 \cdot 10^{-4}$	m^2
Case external radius	$Rout$	0.075	-	m
Bore radius	R_{b}	0.0375	0.0480	m
Teeth and winding mean radius	R_{w}	0.0472	0.0580	m
Back iron mean radius	R_{y}	0.0597	0.0700	m
External case mean radius	R_{h}	0.0663	-	m
Copper slot fill	α	0.565	-	-
Mass of copper windings	m_{w}	2.355	-	kg
Mass of polymer insulation	m_{ins}	1.055	-	kg
Mass of external case	m_{h}	2.857	-	kg
Mass of teeth body	m_{teeth}	1.812	2.386	kg
Mass of stator back iron	m_{y}	1.703	2.624	kg
Copper Young's modulus	E_{c}	$110 \cdot 10^9$	-	Pa
Core lamination Young's modulus	E_{w}	$200 \cdot 10^9$	$200 \cdot 10^9$	Pa
Case Young's modulus	E_{h}	$69 \cdot 10^9$	-	Pa

B. Equation of motion

Fig. 7 depicts the free body diagram of an infinitesimal angular portion $d\theta$ of the curved beam of Fig. 5b, where all the external loads, internal actions and inertia forces are reported, as well as the radial, $u = u(\theta, t)$, and tangential, $w = w(\theta, t)$ displacements of the beam.

By computing the three equilibrium equations (direction t, direction n and rotation θ in Fig. 7) the following relations are obtained

$$S = -\bar{p}R - \frac{\partial N}{\partial \theta} + \rho AR \cdot \frac{\partial^2 w}{\partial t^2} \tag{9a}$$

$$\frac{\partial S}{\partial \theta} = N - \bar{f}R + \rho AR \cdot \frac{\partial^2 u}{\partial t^2} \tag{9b}$$

$$S = \frac{1}{R}\frac{\partial M}{\partial \theta} + q \tag{9c}$$

Substituting eq. 9c in eq. 9b and deriving with respect to θ leads to

$$\frac{1}{R}\frac{\partial^3 M}{\partial \theta^3} + \frac{\partial^2 q}{\partial \theta^2} = \frac{\partial N}{\partial \theta} - \frac{\partial \bar{f}}{\partial \theta}R + \rho AR\frac{\partial^2}{\partial t^2}\frac{\partial u}{\partial \theta} \tag{10}$$

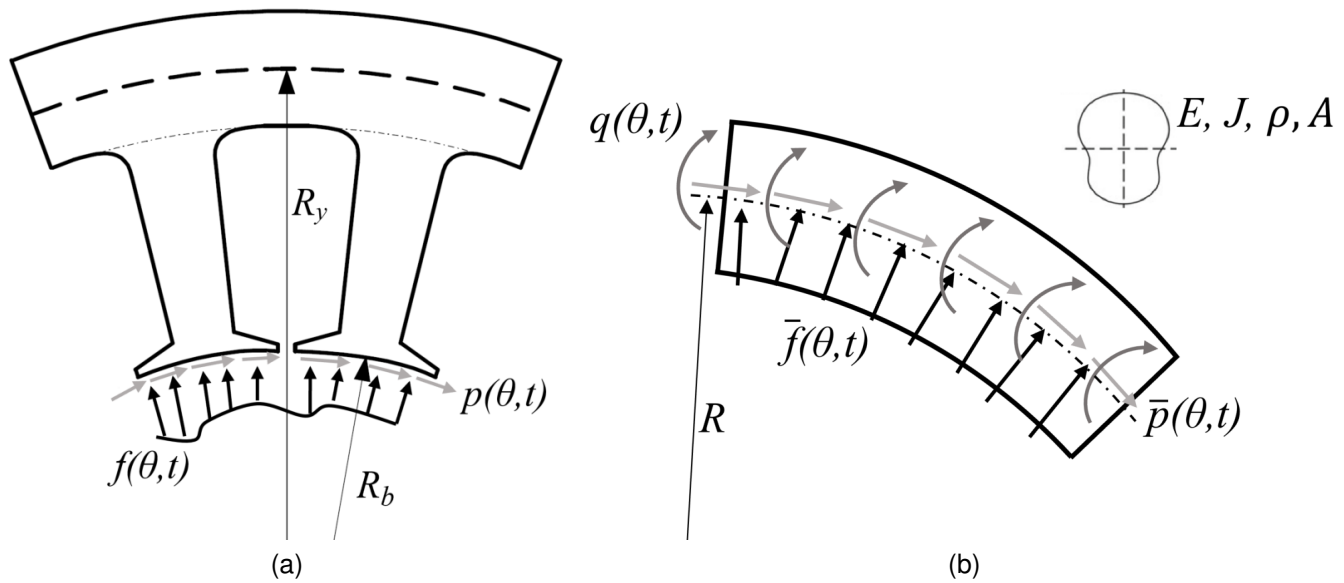

Fig. 5. Simplified analytical model for stator vibration. (a) Scheme of applied electromagnetic force density. (b) Equivalent curved beam approximation.

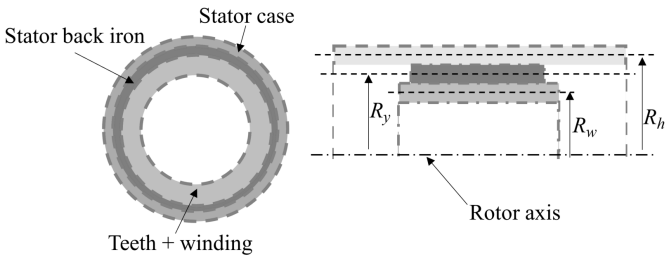

Fig. 6. Scheme of the three main regions of the stator.

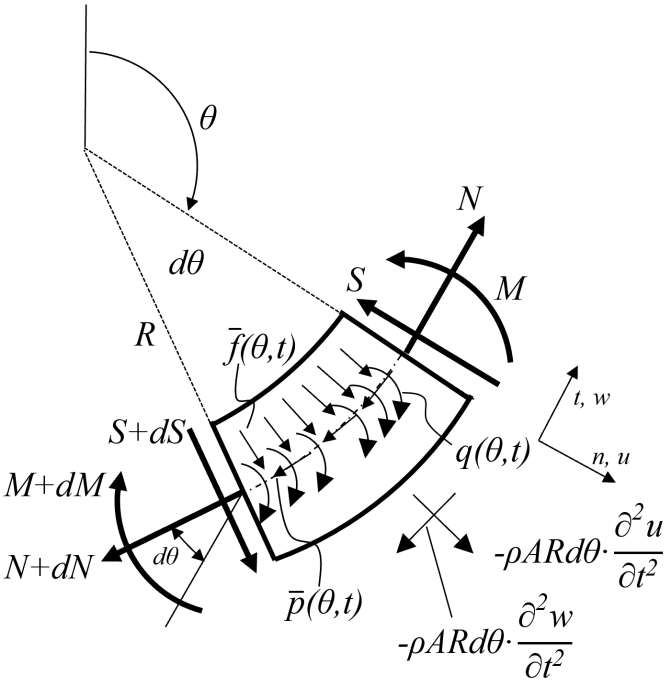

Fig. 7. Free body diagram of an infinitesimal portion of the curved beam.

and replacing eq. 9a in eq. 10 the following relation is obtained

$$\frac{1}{R}\frac{\partial^3 M}{\partial \theta^3} + \frac{\partial^2 q}{\partial \theta^2} = -\bar{p}R - \frac{1}{R}\frac{\partial M}{\partial \theta} - q + \rho AR\frac{\partial^2 w}{\partial t^2} - \frac{\partial \bar{f}}{\partial \theta}R + \rho AR\frac{\partial^2}{\partial t^2}\frac{\partial u}{\partial \theta} \tag{11}$$

Assuming small displacements and conservation of the total length of the beam, the following additional compatibility conditions are derived [27], [28]

$$M = -\frac{EJ}{R^2}\left(u + \frac{\partial^2 u}{\partial \theta^2}\right) \tag{12a}$$

$$\frac{\partial w}{\partial \theta} = -u \tag{12b}$$

Finally, replacing eqs. 12a and 12b in eq. 11, the equation of motion of the curved beam reads

$$\frac{\partial^6 u}{\partial \theta^6} + 2\frac{\partial^4 u}{\partial \theta^4} + \frac{\partial^2 u}{\partial \theta^2} - \frac{R^4}{EJ}\left(\frac{\partial \bar{p}}{\partial \theta} + \frac{\partial^2 \bar{f}}{\partial \theta^2} + \frac{1}{R}\frac{\partial^3 q}{\partial \theta^3} + \frac{1}{R}\frac{\partial q}{\partial \theta}\right) = -\frac{\rho AR^4}{EJ}\cdot\frac{\partial^2}{\partial t^2}\left(-u + \frac{\partial^2 u}{\partial \theta^2}\right) \tag{13}$$

Eq. 13 is consistent with the one reported in [28], with the addition of the term q, which accounts for the stator tooth lever arm.

C. Free vibration

The solution of the free vibration of the ring are calculated by setting the loading terms of eq. 13 (namely $\bar{f}$,$\bar{p}$ and q) to zero and assuming a harmonic solution

$$u(\theta, t) = U \cdot e^{i(n\theta + \omega_n t)} \tag{14}$$

the natural frequencies ω_n (under free boundary conditions) can be obtained by solving the characteristic equation, and read

$$\omega_n^2 = \frac{EJ}{\rho AR^4}\cdot\frac{n^6 - 2n^4 + n^2}{n^2 + 1} \qquad n = 2, 3, 4, ... \tag{15}$$

D. Forced vibration

Given the nature of the load (eq. 2), the steady-state overall response of the system can be expressed as a superposition of the responses to each single harmonic load

$$u(\theta,t)=\sum_{n=-\infty}^{+\infty}\sum_{k=-\infty}^{+\infty}\left(Y_{n,k}^{\mathrm{r}}+Y_{n,k}^{\tau}\right)\cdot e^{i(n\theta+k\omega_0 t)} \tag{16}$$

where $Y_{n,k}^{\mathrm{r}}$ and $Y_{n,k}^{\tau}$ are the $n-k$ (complex) harmonic amplitudes of the radial displacement due to the radial and tangential forces, respectively.

Replacing the forced solution of eq. 16 into eq. 13, and separating the effects of radial and tangential forces the following is obtained

$$Y_{n,k}^{\mathrm{r}}=\frac{F_{n,k}}{\rho A\omega_n^2}\cdot\frac{R_b}{R}\cdot\frac{n^2}{n^2+1}\cdot\eta_{n,k} \tag{17a}$$

$$Y_{n,k}^{\tau}=-\frac{P_{n,k}\cdot i}{\rho A\omega_n^2}\cdot\frac{R_b}{R}\cdot\frac{n}{n^2+1}\cdot\left[1+\frac{R-R_b}{R}\cdot\left(n^2-1\right)\right]\cdot\eta_{n,k} \tag{17b}$$

where the terms $\eta_{n,k}$ are the modal amplification factors

$$\eta_{n,k}=\frac{1}{1-\left(\dfrac{k\omega_0}{\omega_n}\right)^2+2\cdot\xi\cdot i\cdot\left(\dfrac{k\omega_0}{\omega_n}\right)} \tag{18}$$

with ξ being the modal damping ratio, assumed constant and equal to 0.01 for all the modes.

The results obtained in eqs. 17a and 17b are in accordance with those reported in [28], with the addition of the second term in square brackets of eq. 17b, which accounts for the tooth lever arm effect. An example of a simulated 2D spectrum of the radial vibration amplitude for the two considered motors is shown in Fig. 8. In particular, for Motor 1 the result refers to a rotational speed of 1440 rpm and a torque of 26 Nm (Fig. 8a), while for Motor 2, open circuit condition at a revolution speed of 700 rpm are simulated (Fig. 8b). Both for the two considered motors, the structural vibration is highly dominated by order 2 harmonics, typical of the 10-pole/12-slot topology [20].

E. Acoustic model

Once the radial displacement field is computed, the acoustic emission of the motor can be estimated. The stator surface is modeled as an infinitely long cylinder (Fig. 9) with radius equal to R_{out} (see TABLE II). For this particular case, analytical solutions of the radiated sound pressure field can be found in the literature [18], [19]; in particular, assuming a uniform radial vibration distribution along the axial direction, the acoustic sound pressure field reads

$$s(r,\theta,t)=\Re\Big(\sum_{n=-\infty}^{+\infty}\sum_{-\infty}^{+\infty}-\frac{i\cdot V_{n,k}\cdot\rho_0 c_0}{k_0\dfrac{dH_n^{(2)}(k_0R_{\mathrm{out}})}{d(k_0R_{\mathrm{out}})}}\cdot H_n^{(2)}(k_0r)\cdot e^{i(n\theta+k\omega_0 t)}\Big) \tag{19}$$

where ρ_0 and c_0 are the air density and sound speed, respectively, $k_0=\dfrac{k\omega_0}{c_0}$ is the acoustic wavenumber and $H_n^{(2)}$ is the 2^{nd} kind Hankel function of order n. The terms $V_{n,k}$ in eq. 19 are the (n,k) harmonic amplitudes of the radial velocity of the surface, which can be obtained by time-derivation of eq. 16.

TABLE III
COMPARISON OF THE NATURAL FREQUENCIES OBTAINED FROM THE ANALYTICAL MODEL AND THE EXPERIMENTAL TESTS ON MOTOR 1 [10].

Space order	Analytical	Experimental	Percent difference
Mode 2	1720 Hz	1729 Hz	0.5 %
Mode 3	3378 Hz	3502 Hz	3.5 %
Mode 4	6477 Hz	5974 Hz	8.4 %

TABLE IV
COMPARISON OF THE NATURAL FREQUENCIES OBTAINED FROM THE ANALYTICAL MODEL AND THE EXPERIMENTAL TESTS ON MOTOR 2 [24].

Space order	Analytical	Experimental	Percent difference
Mode 2	572 Hz	720 Hz	25.8 %
Mode 3	1619 Hz	1495 Hz	8.3 %
Mode 4	3100 Hz	2424 Hz	27.8 %

IV. RESULTS

In this section, the proposed analytical model is validated comparing the computed natural frequencies and vibration levels of the two considered motors with their respective experimental data reported in the related papers [10], [24].

Secondly, the results of acoustic prediction are presented.

A. Model validation

1) Natural frequencies: TABLE III reports a comparison between the natural frequencies calculated with the model and those obtained from modal testing. The analytical model is accurate in estimating low-order modes. At high order deformation mode, the percent difference increases. The same comparison is done for Motor 2, and results are shown in TABLE IV. In the case of Motor 2 the correlation with experimental natural frequency is worse, with differences higher than 25% in some cases. The motivation could lie in the atypical construction of Motor 2, that features a stator lamination stack hold together and fixed to the test bench by means of only four bolts passing trough the whole axial stack length. This solution is certainly less stiff than conventional constructions (stack lamination fit inside an external metallic case) and is strongly dependent on the amount of preload that is given to the fixing bolts.

2) Forced vibration: Fig. 10 shows the computed spectrum of the radial velocity on the external surface of Motor 1 running at 1440 rpm and 26 Nm along with the experimental data. Numerical simulations have been performed both including and excluding (circle markers and cross markers in Fig. 10) the effect of tangential forces. As clearly shown in Fig. 10, in case such forces are neglected vibration levels are about 50-60% lower.

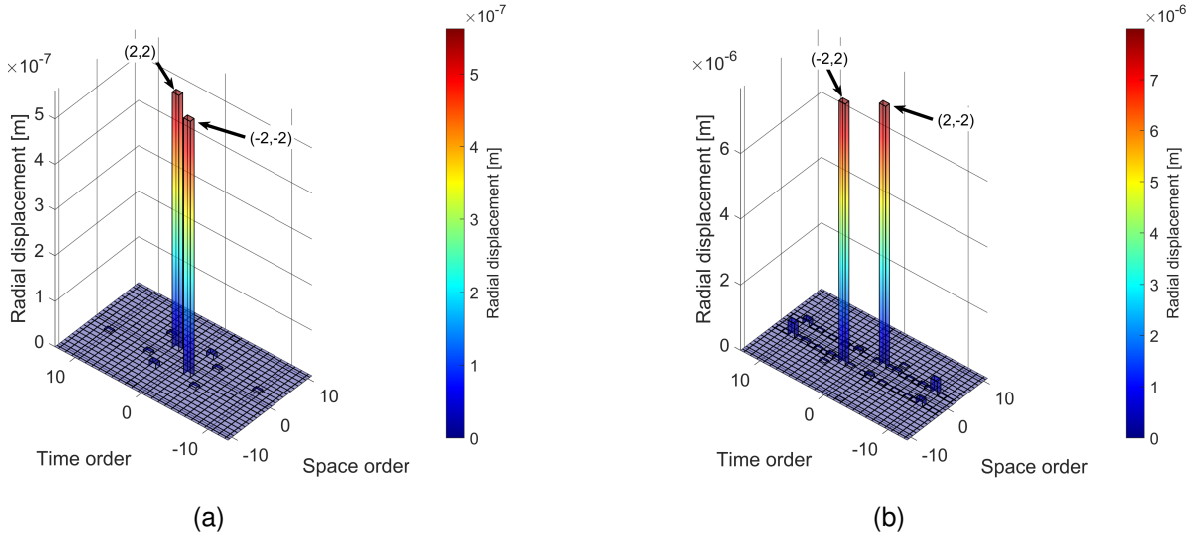

Fig. 8. Spectrum of the radial vibration of the two considered motors. (a) Motor 1, 26 Nm, 1440 rpm. (b) Motor 2, open circuit, 700 rpm.

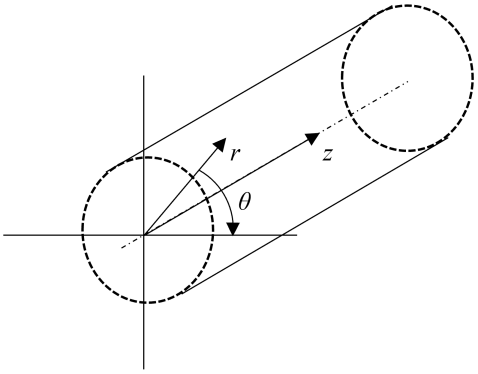

Fig. 9. Infinitely long cylindrical radiator acoustic model.

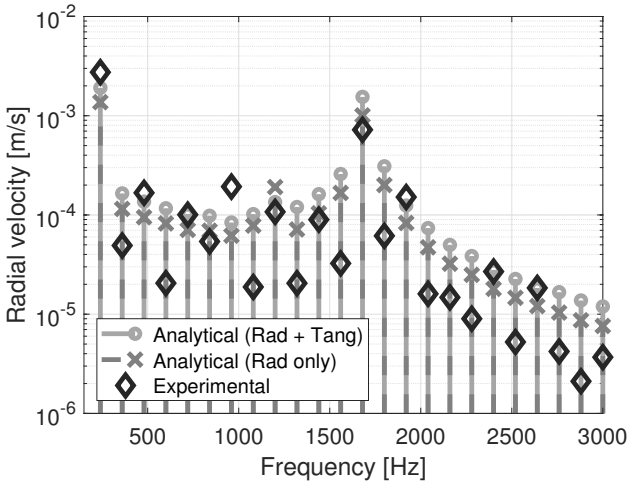

Fig. 10. Spectrum of radial velocity amplitude of a point on the outer surface of the case (working point: 1440 rpm - 26 Nm). Gray circles: analytical model with combined effect of radial and tangential forces. Gray X markers: analytical model with radial forces only. Black markers: experimental data extracted from [10].

Both simulation and experiment show two main harmonic components at 240 and 1680 Hz respectively. The first one is mainly given by the combination of orders (2,2) and (10,2) in the force spectra (see Fig. 1). The second highest peak is located at 1680 Hz, close to the natural frequency of mode 2 (see TABLE III), which explains the high vibration level in this region.

Both the two peaks are well approximated by the analytical model, in particular, for the highest peak (240 Hz) the analytical model with effect of tangential forces is underestimating the peak of about 30 %, the difference rises up to 49 % if the contribution of tangential forces is neglected. For the second peak (1680 Hz), the analytical model is overestimating the velocity amplitude of about 50 %, while with only the contribution of radial forces the difference is reduced to 30 %. In any case, the limited percentage difference between the model and the experimental confirms an reasonable level of accuracy of the proposed simplified model.

The experimental data reported in Fig. 10 show additional localised peaks at different frequencies, while the analytical model exhibits a smoother trend. This can be explained by the effect of axial vibration modes, which are neglected by the analytical model.

Concerning Motor 2, a velocity sweep from 200 to 1200 rpm in open circuit conditions has been simulated and compared with available experimental acquisitions [24]. In this condition, the electric motor was simply driven by an external motor and vibration was measured by means of a series of accelerometers mounted on the external surface of the motor back iron (see [24] for details). The simulated spectrogram is shown in Fig. 11, where orders 2, 4, 6, 8 and 10 are highlighted. Simulations were done either considering only radial electromagnetic forces (Fig. 11b) or combining the effects of radial and tangential ones (Fig. 11a). Simulated results are consistent with the experimental ones shown in Fig. 11c, both in terms

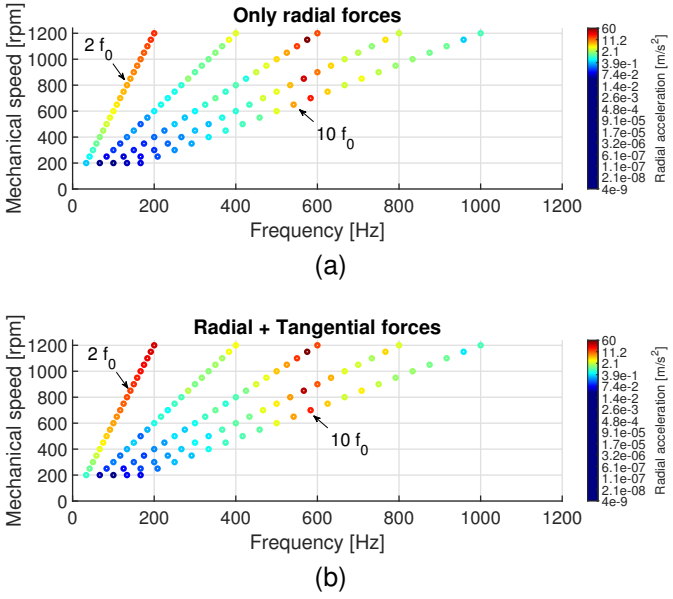

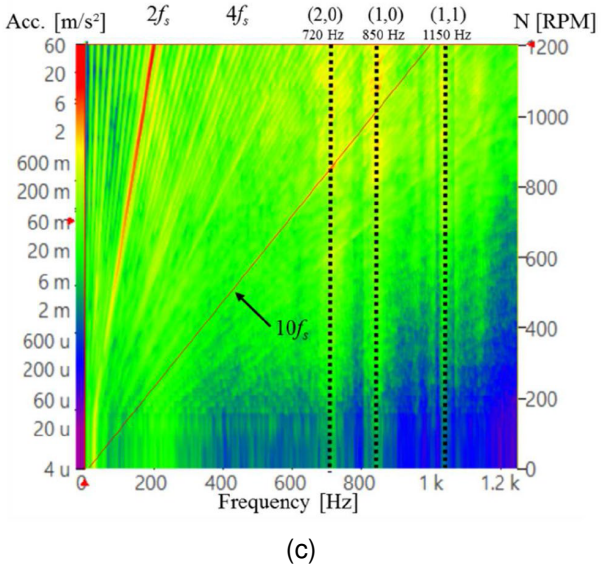

Fig. 11. Spectrogram of simulated and measured radial acceleration on the surface of Motor 2, open circuit conditions. (a) Effect of only radial forces. (b) Combined effect of radial and tangential forces. (c) Experimental data, adapted from [24].

of acceleration levels and main harmonic contributions. In particular simulations show that the effect of order 2 is dominating over the whole range of rotational speeds, with a continuous increase with the motor speed, which is confirmed by the experimental acquisitions (Fig. 11c). Order 10, on the other hand, seems to have a peak around 700 rpm, where the frequency of the electromagnetic forces matches the natural frequency of deformation mode 2 (572 Hz, see TABLE IV). The same happens also in the experimental data, where in this case the peak is shifted upwards around 850 rpm, which is a consequence of the error of the analytical model in the estimation of mode 2 frequency (see TABLE IV).

Finally, the comparison of Fig. 11a and Fig. 11b confirms also for Motor 2 the important effect of tangential forces in the vibration levels (almost 50-60%), especially on order 2.

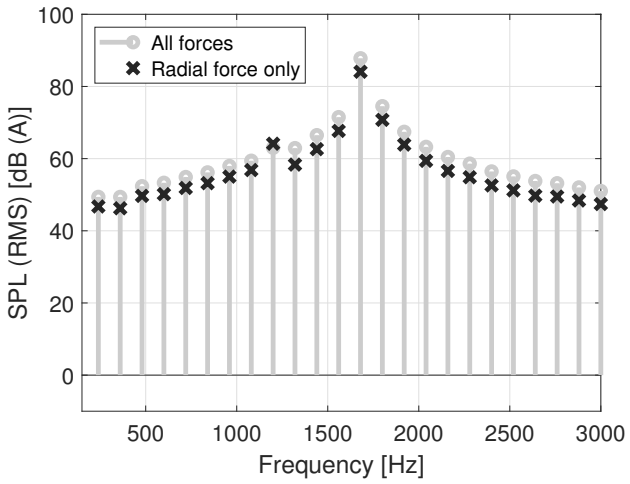

Fig. 12. Spectra of simulated SPL at a distance of 60 mm from the surface considering all forces (gray lines) and radial force only (black markers).

B. Acoustic emission

The total sound pressure time history at any point near the motor surface can be calculated by applying eq. 19. The sound pressure level (SPL) is used as noise emission indicator and can be derived once the sound pressure time history is available

$$SPL = 20 \cdot \log_{10}\left(\frac{[s]_{\mathrm{RMS}}}{2 \cdot 10^{-5}}\right) \tag{20}$$

The harmonic content of the SPL level at a distance of 60 mm from the surface of Motor 1 calculated by the analytical model is shown in Fig. 12. In the figure, both the results obtained for all forces and for radial force only are displayed. The two spectra show a main harmonic contribution to the acoustic emission at 1680 Hz, mainly caused by the high vibration levels introduced by mode 2. As expected, when all the electromagnetic force contributions are included, the sound levels are higher than those computed when only the radial forces are accounted for. The difference between the two calculated SPLs sets around 3 dB(A) for the maximum peak, nearly equivalent to a 50% reduction of the sound pressure amplitude. This result is fully consistent with [10], where the authors found a comparable reduction of the simulated vibration levels in case tangential forces were neglected.

Regarding Motor 2, the simulated spectrograms of the acoustic emission are shown in Fig. 13a and Fig. 13b, where each graph depicts the result considering radial forces only and the combined effect of radial and tangential ones respectively. As for Motor 1, the addition of the tangential force contribution provides an increase of the acoustic emission of about 3-4 dB(A), that involves mainly order 2 harmonics.

V. Discussion

The rapid ongoing shift in the vehicle technology from conventional to electric powertrains is proposing new and hard challenges to vehicle engineers, who cannot count any more on the experience maturated over decades of research and development. In this framework, it is of crucial importance

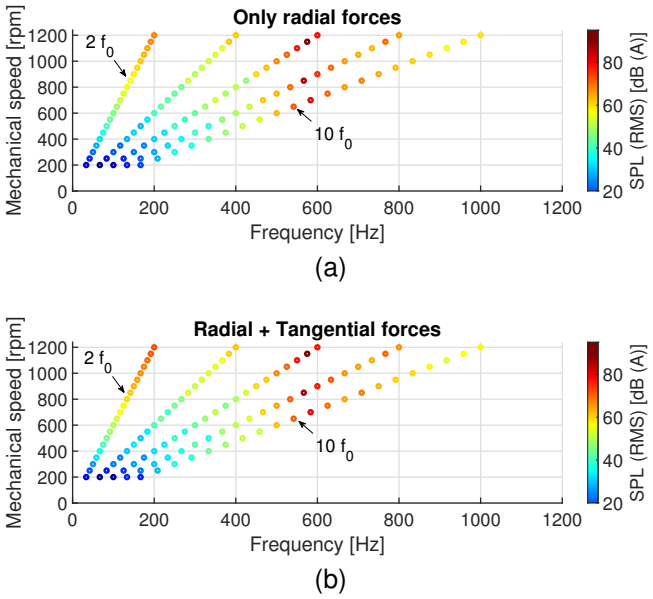

Fig. 13. Spectrogram of simulated acoustic emission at a distance of 60 mm from the surface of Motor 2, open circuit conditions. (a) Effect of only radial forces. (b) Combined effect of radial and tangential forces.

to take winning decisions at the beginning of the design process. The design of innovative electric powertrains makes no exception.

Complex numerical models allow to get a highly accurate estimation of the response of electric machines, but require a large number of input data and parameters, generally not available at the very beginning of the design process.

The proposed analytical model provides explicit mathematical relations between (few) main parameters related to the structure and to the topology of the electric machine and its NVH response. This enables design engineers to derive preliminary results within a very short time and with a limited set of input parameters. The model was developed specifically to be used with PMSMs and represents a useful tool for designers, who can select the best topology of the electric machine including also NVH requirements. The proper selection of the machine layout very often makes the difference for a successful product.

Being the model quite general, it can be extended to different types of electric machines (even induction motors), provided that input force spectra are available.

Explicit analytical expressions of the NVH response of the machine by including the effect of tangential electromagnetic forces have been derived. The contribution of tangential forces, normally neglected in current state of the art analytical methods, is generally evaluated through numerical approaches.

The obtained analytical expressions reveal at first that tangential effects may be of the same order of magnitude of radial ones and therefore need to be included to have a more accurate prediction of the response of the motor. Secondly, they allow to formulate the following simple, but general rules of thumb that may have important practical implications for design engineers.

- From eq. 17b it emerges that the effect of the tangential forces (first term in square bracket) tends to decrease like $\frac{1}{n}$, meaning that the effect is progressively vanishing increasing the spatial order
- the term related to the tooth lever-arm (second term in square bracket of eq. 17b), on the contrary, increases linearly with n and is modulated by the term $\frac{R-R_b}{R}$, meaning that, for a fixed reference diameter, the effect of the tangential force on the vibration amplitude increases with the increase of the tooth height [10].
- the presence of low (space-) order harmonics in the electromagnetic forces can be detrimental for the NVH performances of the machine, as they could excite low order deformation modes near the resonance region.

VI. Conclusions

In the paper, a simplified analytical method for NVH modelling of PMSMs is presented. The model relies on an elastic circular beam loaded by radial and tangential electromagnetic force distributions. The harmonic decomposition of the Maxwell stress tensor in the air-gap is used as exciting force. Explicit analytical expressions of the vibration response of the beam to a single space- and time- harmonic load contribution have been derived. The overall vibration is then reconstructed by applying the superposition principle.

The vibrational model has been benchmarked against two sets of experimental data extracted from the literature, both referring to a 10-pole/12-slots machine configuration.

The calculated velocity field is eventually used as input for the acoustic analysis: the analytical closed-form solutions of the sound pressure field around the structure have been obtained by applying the cylindrical sound radiators theory.

The effect of tangential forces on the acoustic emission has been analysed, showing a contribution of about 50% on the amplitude of the acoustic pressure for both the motors considered.

The derived analytical expressions show that the presence of low-order harmonics in the electromagnetic forces may be detrimental for the NVH performance of PM motors as they could excite structural modes near the resonance, especially in case of machines with a high number of pole pairs. This is a simple, but useful, general design rule to remember during the concept phase.

The developed model is not intended to replace the more accurate yet complex FE modeling, but to be a prompt and quick tool to be used by design engineers for preliminary assessments. The model has proven to be useful to correlate basic structural and topological parameters of motors to their NVH performances.

Acknowledgements

The authors wish to thank Eng. Federico Citroni and Eng. Alberto Cocchi for the support given in the implementation of the electromagnetic model.

The authors would also acknowledge scientists from [10] and [24]. These latter, in particular, for having shared raw data for the computational of the air-gap forces.

REFERENCES

[1] The European Commission, *'Fit for 55': delivering the EU's 2030 Climate Target on the way to climate neutrality*. COM/2021/550, 2021.

[2] https://www.acea.auto/, accessed: Feb 2022.

[3] https://clepa.eu/, accessed: Feb 2022.

[4] http://www.evs32.org/, accessed: Feb 2022.

[5] W. Deng and S. Zuo, "Electromagnetic vibration and noise of the permanent-magnet synchronous motors for electric vehicles: An overview," *IEEE Transactions on Transportation Electrification*, vol. 5, no. 1, pp. 59–70, 2019.

[6] B. Bilgin, J. Liang, M. V. Terzic, J. Dong, R. Rodriguez, E. Trickett, and A. Emadi, "Modeling and Analysis of Electric Motors: State-of-the-Art Review," *IEEE Transactions on Transportation Electrification*, vol. 5, no. 3, pp. 602–617, 2019.

[7] J. Zou, H. Lan, Y. Xu, and B. Zhao, "Analysis of Global and Local Force Harmonics and Their Effects on Vibration in Permanent Magnet Synchronous Machines," *IEEE Transactions on Energy Conversion*, vol. 32, no. 4, pp. 1523–1532, 2017.

[8] S. Wang, H. Jianfeng, Y. Sun, and H. Cao, "Analysis and Reduction of Electromagnetic Vibration of PM Brush DC Motors," *IEEE TRANSACTIONS ON INDUSTRY APPLICATIONS*, vol. 55, no. 5, pp. 4605–4612, 2019. [Online]. Available: http://www.ieee.org/publications_standards/publications/rights/index.html

[9] F. Lin, S. Zuo, W. Deng, and S. Wu, "Modeling and Analysis of Electromagnetic Force, Vibration, and Noise in Permanent-Magnet Synchronous Motor Considering Current Harmonics," *IEEE Transactions on Industrial Electronics*, vol. 63, no. 12, pp. 7455–7466, 2016.

[10] H. Lan, J. Zou, Y. Xu, and M. Liu, "Effect of Local Tangential Force on Vibration Performance in Fractional-Slot Concentrated Winding Permanent Magnet Synchronous Machines," *IEEE Transactions on Energy Conversion*, vol. 34, no. 2, pp. 1082–1093, 2019.

[11] Y. Fang and T. Zhang, "Vibroacoustic Characterization of a Permanent Magnet Synchronous Motor Powertrain for Electric Vehicles," *IEEE Transactions on Energy Conversion*, vol. 33, no. 1, pp. 272–280, 2018. [Online]. Available: http://ieeexplore.ieee.org.

[12] E. Devillers, M. Hecquet, J. Le Besnerais, and M. Régniez, "Tangential Effects on Magnetic Vibrations and Acoustic Noise of Induction Machines using Subdomain Method and Electromagnetic Vibration Synthesis," in *2017 IEEE International Electric Machines and Drives Conference (IEMDC)*, 2017, pp. 1–8.

[13] D. Torregrossa, F. Peyraut, B. Fahimi, J. Mboua, and A. Miraoui, "Multiphysics finite-element modeling for vibration and acoustic analysis of permanent magnet synchronous machine," *IEEE Transactions on Energy Conversion*, vol. 26, no. 2, pp. 490–500, 2011.

[14] F. Lin, S. Zuo, W. Deng, and S. Wu, "Noise Prediction and Sound Quality Analysis of Variable-Speed Permanent Magnet Synchronous Motor," *IEEE TRANSACTIONS ON ENERGY CONVERSION*, vol. 32, no. 2, pp. 698–706, 2017. [Online]. Available: http://ieeexplore.ieee.org.

[15] F. Chai, Y. Li, Y. Pei, and Z. Li, "Accurate modelling and modal analysis of stator system in permanent magnet synchronous motor with concentrated winding for vibration prediction," *IET Electric Power Applications*, vol. 12, no. 8, pp. 1225–1232, 2018.

[16] S. Zuo, F. Lin, and X. Wu, "Noise Analysis, Calculation, and Reduction of External Rotor Permanent-Magnet Synchronous Motor," *IEEE Transactions on Industrial Electronics*, vol. 62, no. 10, pp. 6204–6212, 2015.

[17] P. Kotter, D. Morisco, M. Boesing, O. Zirn, K. Wegener, and R. B. Gmbh, "Noise-Vibration-Harshness-Modeling and Analysis of a," *IEEE Transactions on Magnetics*, vol. 54, no. 3, pp. 3–6, 2018.

[18] B. Weilharter, O. Biro, H. Lang, G. Ofner, and S. Rainer, "Validation of a comprehensive analytic noise computation method for induction machines," *IEEE Transactions on Industrial Electronics*, vol. 59, no. 5, pp. 2248–2257, 2012.

[19] J. Gieras, C. Wang, and J. Lai, *Noise of polyphase electric motors*. Taylor and Francis, 2005.

[20] R. Islam and I. Husain, "Analytical model for predicting noise and vibration in permanent-magnet synchronous motors," *IEEE Transactions on Industry Applications*, vol. 46, no. 6, pp. 2346–2354, 2010.

[21] A. McCloskey, X. Arrasate, X. Hernández, I. Gómez, and G. Almandoz, "Analytical calculation of vibrations of electromagnetic origin in electrical machines," *Mechanical Systems and Signal Processing*, vol. 98, pp. 557–569, jan 2018.

[22] M. Boesing and R. W. De Doncker, "Exploring a Vibration Synthesis Process for the Acoustic Characterization of Electric Drives," in *The XIX International Conference on Electrical Machines - ICEM 2010*, 2010, pp. 1–6.

[23] X. Xu, Q. Han, Z. Qin, and F. Chu, "Analytical methods for the radial electromagnetic vibration of stator in permanent magnet motors with an amorphous alloy core," *Mechanical Systems and Signal Processing*, vol. 145, nov 2020.

[24] E. Devillers, K. Degrendele, M. Hecquet, J. P. Lecointe, J. Le Besnerais, and G. Cousin, "Open-Access Testbench Data for NVH Benchmarking of E-Machines under Electromagnetic Excitations," in *SAE Technical Papers*, vol. 2019-June, no. June, 2019, pp. 1–8.

[25] X. Xu, Q. Han, and F. Chu, "Review of electromagnetic vibration in electrical machines," *Energies*, vol. 11, no. 7, pp. 1779–1811, 2018.

[26] B. Hannon, P. Sergeant, and L. Dupre, "Time- and spatial-harmonic content in synchronous electrical machines," *IEEE Transactions on Magnetics*, vol. 53, no. 3, pp. 1–6, 2017.

[27] F. Ballo, G. Previati, M. Gobbi, and G. Mastinu, "Tire-Rim Interaction, a Semi-Analytical Tire Model," *Journal of Mechanical Design, Transactions of the ASME*, vol. 140, no. 4, p. 041401, 2018.

[28] S. S. Rao, *Vibration of Continuous Systems*. John Wiley and Sons, INC., 2007. [Online]. Available: http://www.wiley.com/go/permissions.

Federico Ballo got the Ph.D. degree in Mechanical Engineering at Politecnico di Milano (Italy) in 2015 and is currently employed as a Research Fellow in the same institution. His main research interests are: Multi-Objective optimization of complex systems, structural optimization, numerical modelling of mechanical systems, with particular reference to ground vehicles

Massimiliano Gobbi received the master's degree (with Hons.) in mechanical engineering and the Ph.D. degree in applied mechanics. He is currently a Full Professor at Politecnico di Milano. In 1998, he was a Visiting Scholar with the Department of Mechanical Engineering, University of California Berkeley. He has authored more than 200 papers. He is the author of 7 international patents and 3 books.

Gianpiero Mastinu received the graduation degree (with Hons.) and the Doctorate degree. He is currently Full Professor at Politecnico di Milano. His scientific activity covers design, construction and test of machines, structures, and mechanical systems with focus on ground vehicles. He is author of five books and 200 papers, Co-Founder of the Laboratory for Safety of Transport Systems.

Roberto Palazzetti graduated in Mechanical Engineering in 2009 and obtained a doctorate in Mechanics of Materials and Technological Processes in 2013, at University of Bologna (Italy). After 5 years as post-doctorate at StrathClyde University in Glasgow (UK), and 3 years as R&D Engineer in a private company, he has been appointed as Associate Professor at Mechanical Engineering Department of Politecnico di Milano (Italy).